The Astrophysical Journal, 505:473–483, 1998 October 1

A DETERMINATION OF THE SPECTRAL INDEX OF GALACTIC SYNCHROTRON EMISSION IN THE 1–10 GHz RANGE

P. Platania,[1] M. Bensadoun,[2] M. Bersanelli,[1] G. De Amici,[3] A. Kogut,[4] S. Levin,[5] D. Maino,[6] and G. F. Smoot[2]
Received 1997 July 30; accepted 1998 May 6

ABSTRACT

We present an analysis of simultaneous multifrequency measurements of the Galactic emission in the 1–10 GHz range with 18° angular resolution taken from a high-altitude site. Our data yield a determination of the synchrotron spectral index between 1.4 and 7.5 GHz of $\beta_{syn} = 2.81 \pm 0.16$. Combining our data with maps made by Haslam et al. and Reich & Reich, we find $\beta_{syn} = 2.76 \pm 0.11$ in the 0.4–7.5 GHz range. These results are in agreement with the few previously published measurements. The variation of β_{syn} with frequency based on our results and compared with other data found in the literature suggests a steepening of the synchrotron spectrum toward high frequencies, as expected from theory because of the steepening of the parent cosmic-ray electron energy spectrum. Comparison between the Haslam data and the 19 GHz map of Cottingham also indicates a spatial variation of the spectral index on large angular scales. Additional high-quality data are necessary to provide a serious study of these effects.

Subject headings: diffuse radiation — radiation mechanisms: nonthermal

1. INTRODUCTION

The detailed study of radio continuum emission allows a direct evaluation of some important parameters that describe the dynamics and structure of the Galaxy: the mean intensity of the magnetic field, the spectral index of the energy spectrum of cosmic-ray electrons, and the temperature and density of interstellar clouds. Another strong motivation for systematic study of the diffuse Galactic emission arises in conjunction with measurements of the cosmic microwave background (CMB); Galactic emission is one of the main sources of unwanted signal in CMB observations, and it is unavoidable even in satellite measurements. It is therefore very important to understand in detail the spectral and spatial variations of the various components of Galactic emission in order to separate them from those arising from the CMB. For this purpose, an experiment dedicated to measuring the centimeter wavelength (1–10 GHz) Galactic emission with multifrequency measurements was carried out in 1988 at White Mountain, California, as part of a USA-Italy collaboration to measure the spectrum of the CMB in the Rayleigh-Jeans region (Smoot et al. 1985). In this paper, we present these previously unpublished data; because of the lack of Galactic emission surveys in this frequency range, new results in this field are very important.

1.1. *The Galactic Emission*

At frequencies below about 30 GHz, Galactic emission is mainly due to synchrotron emission from cosmic-ray electrons interacting with the Galactic magnetic fields and to thermal bremsstrahlung (free-free) emission. In the frequency range of our experiment, the dominant contribution comes from synchrotron radiation (Fig. 1), with free-free radiation contributing significantly on the Galactic plane. Based on the data of Haslam et al. (1982) and Witebsky et al. (1987), we estimate a contribution for the free-free emission of ~30% at 1.5 GHz and ~50% at 7.5 GHz on the Galactic plane.

Our goal has been to determine a mean synchrotron spectral index and its possible variation with frequency. The synchrotron emission arises from relativistic cosmic-ray electrons moving in the Galactic magnetic fields; for an electron population with energy distribution $N(E)$, described by a power law

$$N(E)dE \propto E^{-\delta}\,dE\ , \tag{1}$$

the ensemble synchrotron radiation spectrum in terms of brightness temperature is also a power law,

$$T(\nu) \propto \nu^{-\beta}\ , \tag{2}$$

where ν is the radiation frequency and $\beta = (\delta + 3)/2$. In the energy range $2 \lesssim E \lesssim 15$ GeV (corresponding to frequencies between 408 MHz and 10 GHz for $B \simeq 2.5\ \mu$G), the spectral index of the energy distribution of the cosmic-ray electrons is $\delta \sim 3$ (Bennet et al. 1992), equivalent to $\beta \sim 3$. For higher electron energies, the energy spectrum steepens, and so does the radiation spectrum (Banday & Wolfendale 1991).

The brightness temperature distribution depends on the electron density along the line of sight $N(E, l)$ and on the power P emitted by an electron of energy E into a magnetic field B,

$$T(\nu) \propto \iint P(\nu, B, E)N(E, l)dE\,dl\ . \tag{3}$$

Because of the dependence of B and $N(E)$ on position in the Galaxy, one also expects T and β to be functions of the position in the sky.

2. THE EXPERIMENT

Our analysis is based upon a set of data collected during three nights (1988 September 6, 8, and 10) at the White

[1] Istituto di Fisica Cosmica, Consiglio Nazionale delle Ricerche, via Bassini 15, 20133 Milano, Italy.
[2] Space Science Laboratory and Lawrence Berkeley Laboratory, M/S 50-205, University of California, Berkeley CA 94720.
[3] TRW, Space and Technology Division, R1-2136, 1 Space Park, Redondo Beach CA 90278.
[4] NASA Goddard Space Flight Center, Hughes STX, Code 685, Greenbelt MD 20771.
[5] Jet Propulsion Laboratory, Pasadena CA 91109.
[6] SISSA, International School for Advanced Studies, Strada Costiera 11, 34014, Trieste, Italy.

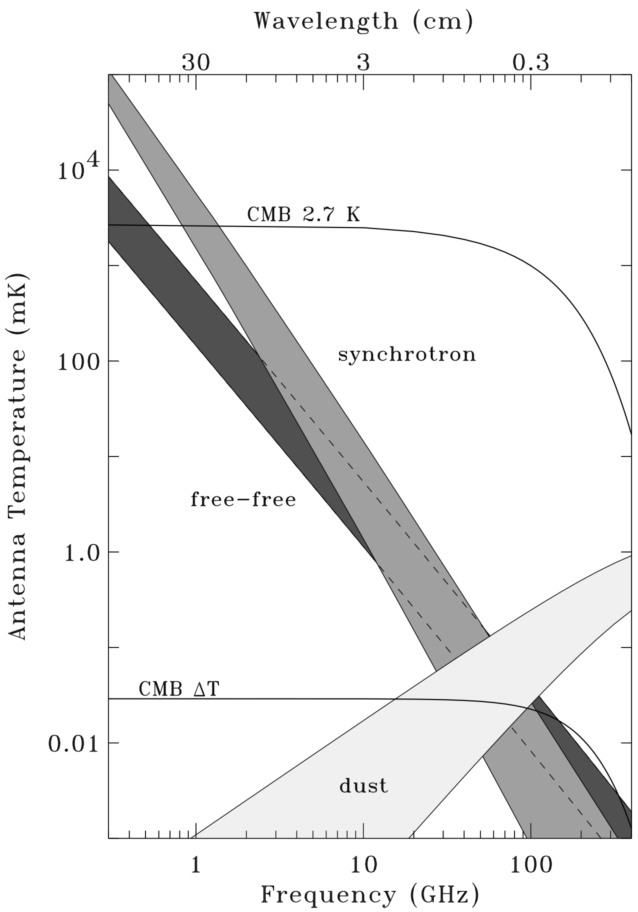

FIG. 1.—Galactic emission components and CMB spectra for moderate angular resolution (7° HPBW) and Galactic latitude $|b| < 20°$. The shaded regions indicate the ranges of synchrotron, free-free, and dust emission. Solid lines indicate the mean CMB spectrum and rms amplitude of the anisotropy.

Mountain Barcroft Station, California (altitude 3800 m, latitude +38; for a review of the entire experiment campaign, see Smoot et al. 1985), with radiometers operating at 1.375, 1.55, 3.8, and 7.5 GHz (Table 1). The instruments are total-power radiometers, whose output signal, S, is proportional to the power, P, entering the antenna aperture. The two lower frequencies were covered by a single radiometer (Bensadoun et al. 1993), which could switch the center frequency of its YIG filter. Details of the 3.8 and 7.5 GHz radiometer can be found in De Amici et al. (1990) and Kogut et al. (1990). Hereafter, the signals are expressed in units of antenna temperature, $T_A = P/kB$, where P is the received power, k is Boltzmann's constant, and B is the bandwidth of the radiometer.

During the Galactic scans, each radiometer was tipped cyclically between 15° to the east and 15° to the west of the zenith, measuring the signal from the sky for 32 s in each position. We took the difference of the signal in these two positions; in this way we were able to cancel, to first order, all the isotropic contributions (CMB and extragalactic sources) and symmetric contributions with respect to the zenith angle (atmospheric and ground emissions). (We consider the CMB as isotropic, since the CMB dipole contribution in the observed region is negligible, less than 2 mK.) The differenced signal can thus be written as

$$T_{A,+15°} - T_{A,-15°} \simeq \Delta T_{A,\mathrm{Gal}} + \delta T , \tag{4}$$

where δT includes the second-order contributions from the other terms and $\Delta T_{A,\mathrm{Gal}}$ is the sum of differential (±15°) synchrotron ($\Delta T_{A,\mathrm{syn}}$) and free-free ($\Delta T_{A,\mathrm{ff}}$) emissions relative to the observed sky regions:

$$\Delta T_{A,\mathrm{Gal}} = \Delta T_{A,\mathrm{syn}} + \Delta T_{A,\mathrm{ff}} . \tag{5}$$

On each night we observed for several hours (see Table 1), thus covering significant sections of the sky, with some overlap and redundancy to check systematic effects.

The experiment was designed to have similar antenna beams for all the radiometers. However, the feeds could not be scaled designs because of mechanical constraints; in particular, the 1.3/1.5 GHz feed was a rectangular horn, corrugated on the east plane (Witebsky et al. 1987), while the feeds at higher frequencies were conical corrugated horns.

Calibration measurements were done every hour during the experiment using the signal from an ambient temperature load (typically $T_{A,\mathrm{amb}} \sim 300$ K) and the zenith sky ($T_{A,\mathrm{zenith}} \sim 4$K). The calibration constant G is

$$G = \frac{T_{A,\mathrm{amb}} - T_{A,\mathrm{zenith}}}{S_{\mathrm{amb}} - S_{\mathrm{zenith}}} , \tag{6}$$

where $T_{A,\mathrm{amb}}$ and S_{amb} are the temperature and the signal, respectively, when the radiometer is looking at the ambient load, and $T_{A,\mathrm{zenith}}$ and S_{zenith} are the temperature and the signal when it looks to the zenith sky. We calibrated the differential signals between the 15° east and 15° west positions using the value of G resulting from the interpolation between adjacent calibration measurements.

TABLE 1

RADIOMETER AND OBSERVATION PARAMETERS

Frequency (GHz)	Measured Sensitivity (mK $\mathrm{Hz}^{-1/2}$)	HPBW[a] (deg)	Date (1988)	R.A. (hr)	Reference[b]
1.375–1.550......	18	18–16	Sep 6	0–4.3, 18.3–24	1
			Sep 8	0–6, 19–24	
3.8...............	13	17	Sep 6	0–4.3, 18.3–24	2
			Sep 8	0–6, 20.3–24	
			Sep 10	21–23	
7.5...............	44	21	Sep 6	0–2.3, 18.3–24	3
			Sep 8	0–6, 19–21	
			Sep 10	21–23	

[a] The HPBW of the Gaussian beam that approximates the measured response.

[b] More details on the experiment can be found in these works.

REFERENCES.—(1) Bensadoun et al. 1993; (2) De Amici et al. 1990; (3) Kogut et al. 1990.

3. DATA ANALYSIS

The integration time is 2 s for all the radiometers; we rejected those points showing occasional spikes and also those immediately following the change in the position of the radiometers. The data were then binned in 4° R.A. intervals, and the differences in equation (4) were calculated, along with their statistical errors.

In order to increase information about the synchrotron spectral index, we compared our data with two sky surveys: the map at 408 MHz of Haslam et al. (1982) and the map at 1420 MHz of Reich & Reich (1986).

Section 3.1 describes data analysis, and § 3.2 describes the procedure we used to make the above maps comparable with our data.

3.1. *Differential Profiles and Corrections*

For a comparison of data taken at different frequencies, we corrected the profiles in order to normalize the responses of the different antennas to our average antenna beam (half-power beam width [HPBW] = 18°). We generated a synthetic sky, representative of synchrotron and free-free emission, as follows: we subtracted the free-free component from the full-sky 408 MHz Haslam et al. (1982) map using a catalog of about 7400 H II sources at 2.7 GHz (C. Witebsky 1978, private communication), scaled to 0.408 GHz with a spectral index $\beta_{\rm ff} = 2.1$, and thus obtained a "pure" synchrotron map. Adopting $\beta_{\rm syn} = 2.8$ and $\beta_{\rm ff} = 2.1$, we scaled the two Galactic components to each of our frequencies; the resulting Galactic maps were convolved to the corresponding radiometer beam at each frequency, and also to the standard resolution HPBW = 18°. We then calculated, for each frequency and for every R.A. bin a in the profiles, the coefficient η needed to convert the measured signal into a signal corresponding to an antenna with 18° HPBW:

$$\eta(a) = \frac{T_{18^\circ}(a)}{T_{\rm HPBW}(a)} , \tag{7}$$

where T_{18° and $T_{\rm HPBW}$ come from the synthetic sky distributions for each frequency. For the points of the differential profile, this translates into the conversion coefficient

$$\eta_{\rm diff} = \frac{\Delta T_{18^\circ}}{\Delta T_{\rm HPBW}} , \tag{8}$$

where

$$\Delta T_{18^\circ} = T_{18^\circ}(a) - T_{18^\circ}(b) = T_{\rm HPBW}(a)\eta(a) - T_{\rm HPBW}(b)\eta(b) , \tag{9}$$

where a and b are generic sky bins whose separation in R.A. is $2^{\rm h}30^{\rm m}$ (in fact, observations of points at 15° from the zenith, carried out at a terrestrial latitude of 38°, correspond to points at hour angles of $\pm 1^{\rm h}15^{\rm m}$ and a declination of 36° on the celestial sphere). Because all the instruments have similar antenna beams, the coefficient $\eta_{\rm diff}$ typically varies in the range 0.8–1, thus giving rise to small corrections to the data.

After this correction, the resulting Galactic profiles are directly comparable, and are shown in Figures 2*a*–2*d*. Note the decreasing signal-to-noise ratio with increasing frequency due to the decreasing Galactic signal, especially the synchrotron component (eq. [2]).

Because the main goal of this work is to evaluate a mean synchrotron spectral index in the observed sky region, for all the profiles the bremsstrahlung contribution has been evaluated using the catalog of H II sources, convolved to the 18° standard antenna beam and scaled to the observation frequencies with a spectral index $\beta_{\rm ff} = 2.1$ (Scheffler & Elsässer 1987). This component has been subtracted to leave just the synchrotron component (see § 4.1 for systematic errors arising from the subtraction).

3.2. *The Maps*

The 408 MHz Haslam et al. (1982) map is a full-sky survey composed from several data sets at the same frequency, obtained using different telescopes with similar beam sizes; the final angular resolution is 0°.85. The 1420 MHz Reich & Reich (1986) map covers declinations $\delta > -19°$ and has an angular resolution of 0°.6. We convolved these surveys with a Gaussian beam with HPBW = 18°, extracted the Galactic profiles corresponding to our observed sky region, and then constructed the differential profiles by simulating the interpretational strategy; the profiles are shown in Figures 2*e* and 2*f*. These two surveys have intrinsic uncertainties in zero-level and gain calibration, the first of which does not affect our analysis because of the differential reduction technique. The gain calibration error is 10% for the 408 MHz map and 5% for the 1420 MHz map; these errors have been added in quadrature to the statistical errors in both map profiles.

The two maps are in total intensity, while our instruments were sensitive only to one linear polarization; to make our data and the maps directly comparable, we corrected the maps using the linear polarization survey of the Galactic background from Brouw & Spoelstra (1976) convolved with the 18° beam. We subtracted from the profiles the component perpendicular to the polarization direction (east-west) of our instruments, yielding profiles at 408 MHz and 1420 MHz that are fully consistent with our observations. In principle, however, because of the effect of Faraday rotation, the resulting estimates of β refer to the particular polarization direction of our instruments. On the other hand, it can be shown that in the frequency range of our measurements, the rotation effect is small. Assuming a typical value of the rotation measure, R, of about 8 rad m^{-2} (Verschuur & Kellermann 1988), we get a rotation of $\phi = R\lambda^2 \simeq 20°$ at 1.355 GHz, leading to a very minor impact ($<0.3\%$) on any evaluations of β in the 1.3–7.5 GHz range. Data involving the 408 MHz map should be considered more carefully because of the large rotation angle induced by Faraday rotation. The polarized component at 408 MHz is at most 5% of the overall signal in the sky region of our measurements. Assuming 100% uncertainty of the rotation angle for a 5% polarized component, we find errors in β of less than 0.06. All the uncertainties introduced by Faraday rotation are included in Table 2. The polarization data have statistical mean errors of 0.34 K for 0.408 GHz and 0.06 K for 1.4 GHz. We included these errors as statistical errors.

Finally, the maps have been corrected for the H II contribution with the same technique used for the new measurements, and errors arising from this procedure were considered.

We also note that Cygnus A, one of the most powerful radio source in the sky, passes directly through our beams near R.A. $\approx 20^{\rm h}$. We want to evaluate the impact of this

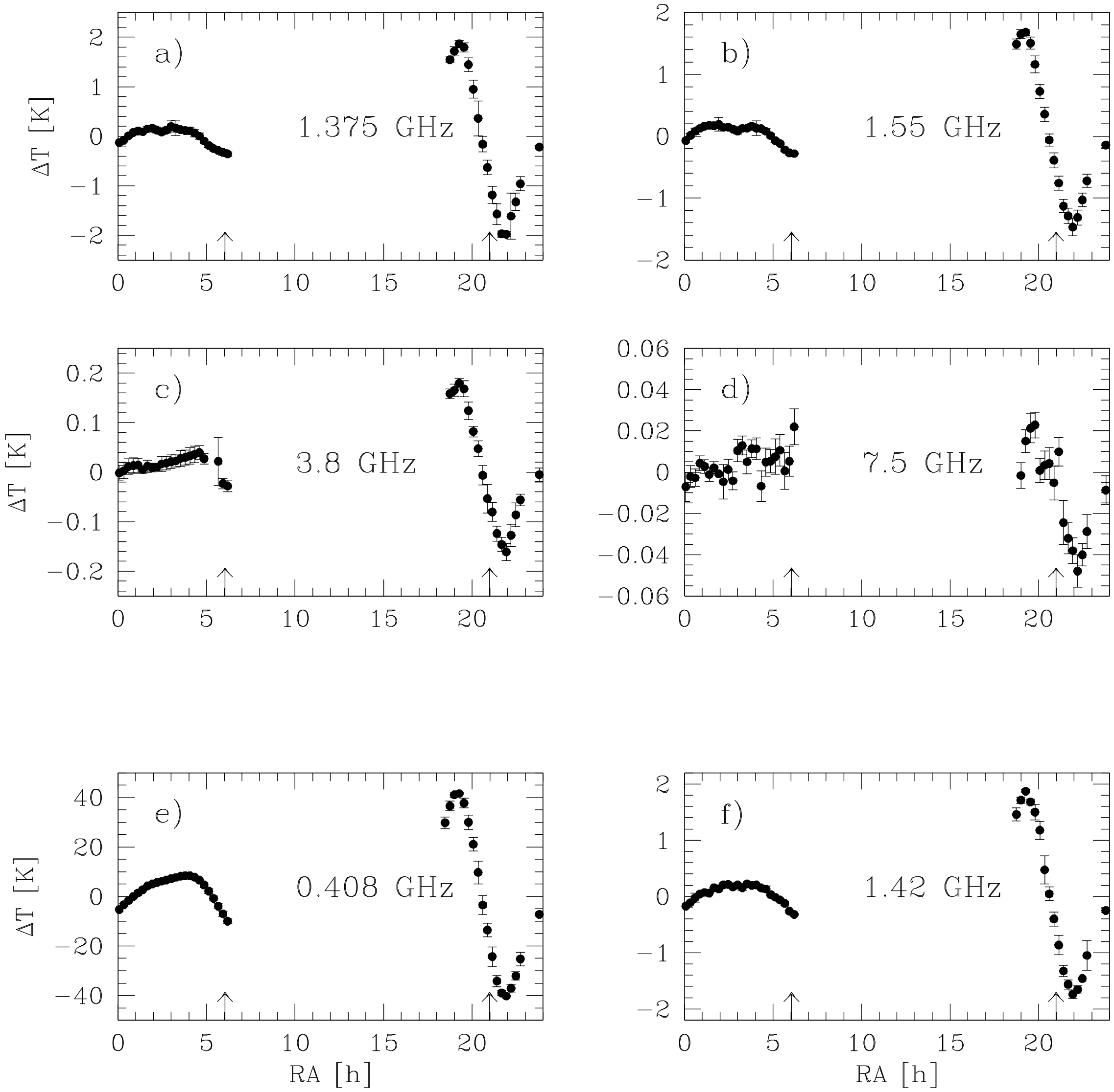

FIG. 2.—All profiles. (*a*)–(*d*): Differential Galactic profiles derived from our data at the frequencies indicated in the plots. (*e*)–(*f*): Differential Galactic profiles derived from the maps at 408 and 1420 MHz. The arrows indicate the points of Galactic plane crossing toward anticenter (5^h) and center (20^h).

source on the determination of the synchrotron spectral index on the angular scale of the experiment ($\lesssim 18°$). From Baars et al. (1977), we derived, in our frequency range, the spectral index for Cyg A, obtaining a value of 3.08 ± 0.06 (between 0.408 and 22 GHz). We calculated the effect on β if we consider Cyg A as a pure synchrotron source, i.e., assuming a spectral index of about 2.8. The variation in our estimation of β is less than 0.02 ($\leq 1\%$). This error is very small, meaning that Cyg A, even as powerful as it is, does not modify our estimation of the synchrotron spectral index on 18° angular scales in a significant way. We included this value in our final error bars.

TABLE 2

SPECTRAL INDICES AND ERRORS

Frequency (GHz)	β_{syn}	$\sigma_{\beta,tot}$
0.408–1.375	2.775	0.111
0.408–1.42	2.776	0.131
0.408–1.55	2.691	0.106
0.408–3.8	2.731	0.085
0.408–7.5	2.951	0.165
1.42–3.8	2.681	0.152
1.42–7.5	3.057	0.252
1.375–3.8	2.689	0.117
1.375–7.5	3.327	0.372
1.550–3.8	2.841	0.110
1.550–7.5	3.609	0.508

4. RESULTS AND ERROR ANALYSIS

In order to evaluate the synchrotron spectral index, we produced temperature-temperature plots, or TT plots. These plots use as ordinate and abscissa antenna temperatures measured simultaneously at two different frequencies on the same region of the sky. Since we have plots with error bars in both coordinates, we fit the data with a general linear least-squares technique (Press et al. 1992). TT plots were made for every pair of frequencies between the data and the maps, excluding 1.375–1.55, 1.375–1.42, and 1.42–1.55 GHz, which are too close to obtain a meaningful result, and 3.8–7.5 GHz, because of the large errors arising from the decreased signal-to-noise ratio. Figure 3 shows all the TT plots; the resulting synchrotron spectral indices are listed in Table 2 with final errors, including the systematic effects discussed in § 4.1. Note the excellent agreement of the

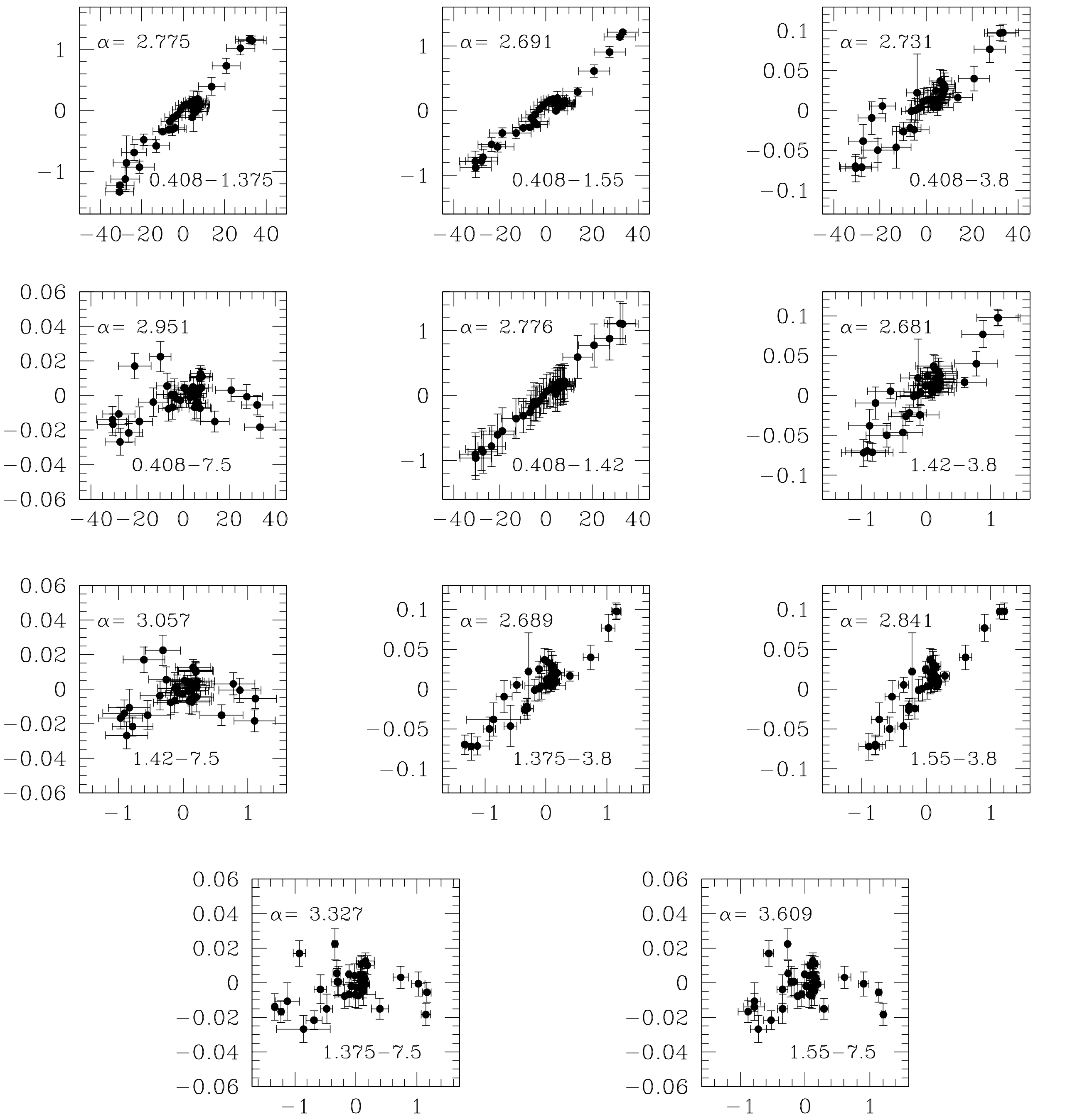

FIG. 3.—All TT plots. The resulting synchrotron spectral index is indicated in each plot, as well as the pair of frequencies (GHz) at which data have been taken, the first referring to the abscissa and the second to the ordinate. The units are K on both axes.

results obtained using low frequencies (1.375 and 1.55 GHz) and the 1.42 GHz map, which confirms that our data have no unexpected systematic problems. The slope of the best fit to the data, m, gives the synchrotron spectral index, $\beta = \log(m)/\log(\nu_1/\nu_2)$, where ν_1 and ν_2 are the frequencies of the two sets of data. Table 3 shows the statistical parameters of the TT plots. Figure 4 shows all our results; the spectral indices are evaluated between the frequency indicated in the box and the frequency on the x-axis. The most significant contribution to the evaluation of β comes from data taken in the region close to the Galactic plane, where there is a large temperature range and thus the most significant contribution to the fit. Thus, our results are primarily representative of synchrotron emission from the Galactic plane.

4.1. *Evaluation of Systematic Effects*

For each of the effects considered in this paragraph, TT plots were used to calculate a spectral index for the data, both with and without a given effect; the difference between the two spectral indices is the induced systematic error on β_{syn}, and we list these in Table 4. In our analysis, we evaluated all the second-order effects producing systematic errors; the discussion is divided into two parts, the first part dedicated to effects arising from corrections in the Galactic profiles, and the second part devoted to the evaluation of instrumental effects.

We consider the possibility that the H II catalog used was not complete, and we have evaluated the effect of this

TABLE 3

STATISTICS

Frequency (GHz)	χ^2_ν [a]	r_S [b]	$N_{\rm points}$ [c]
0.408–1.375......	0.322	0.916	38
0.408–1.42.......	0.031	0.972	38
0.408–1.55.......	0.404	0.874	38
0.408–3.8........	0.620	0.911	38
0.408–7.5........	2.574	0.272	38
1.42–3.8..........	0.396	0.856	38
1.42–7.5..........	2.549	0.252	38
1.375–3.8........	0.956	0.789	38
1.375–7.5........	2.736	0.212	38
1.55–3.8.........	0.917	0.757	38
1.55–7.5.........	2.787	0.190	38

[a] Reduced χ^2 for dof.
[b] Spearman correlation rank coefficient.
[c] Number of data points.

TABLE 4

STATISTICAL AND SYSTEMATIC ERRORS

Frequency (GHz)	$\sigma_{\beta,\rm ff}$	$\sigma_{\beta,\rm ind,ff}$	$\sigma_{\beta,\rm beam}$	$\sigma_{\beta,\rm point}$	$\sigma_{\beta,\rm atm}$	$\sigma_{\beta,\rm stat}$
0.408–1.375......	0.025	0.017	0.032	0.003	0.055	0.064
0.408–1.42.......	0.003	0.033	...	...	0.055	0.100
0.408–1.550......	0.022	0.012	0.039	0.003	0.054	0.060
0.408–3.8........	0.029	0.007	0.025	0.003	0.055	0.041
0.408–7.5........	0.062	0.049	0.002	0.003	0.059	0.130
1.42–3.8..........	0.062	0.034	0.026	0.003	0.054	0.120
1.42–7.5..........	0.123	0.068	0.006	0.003	0.064	0.274
1.375–3.8........	0.028	0.036	0.07	0.003	0.054	0.061
1.375–7.5........	0.129	0.120	0.001	0.003	0.066	0.320
1.550–3.8........	0.033	0.035	0.039	0.003	0.057	0.069
1.550–7.5........	0.185	0.158	0.004	0.004	0.072	0.440

incompleteness on the results. For this purpose, we corrected our data with an earlier catalog of only 900 H II sources and evaluated $\beta_{\rm syn}$; the resulting error, $\sigma_{\beta,\rm ff}$, typically ranges between 0.02 and 0.13, as shown in Table 4. We also took into account the effect produced by an error on the free-free spectral index, considering values $\beta_{\rm ff} = 2.10 \pm 0.05$, typically obtaining an error $\sigma_{\beta,\rm ind,ff}$ in the range 0.01–0.1. We also evaluated all the indices without the subtraction of the H II component; the typical difference between these indices and the corrected ones is 0.3. We estimate that in the worst case, the H II compilation would have 20% error, resulting in an error of $\sim$0.06 in the spectral indices, which would not change the results significantly.

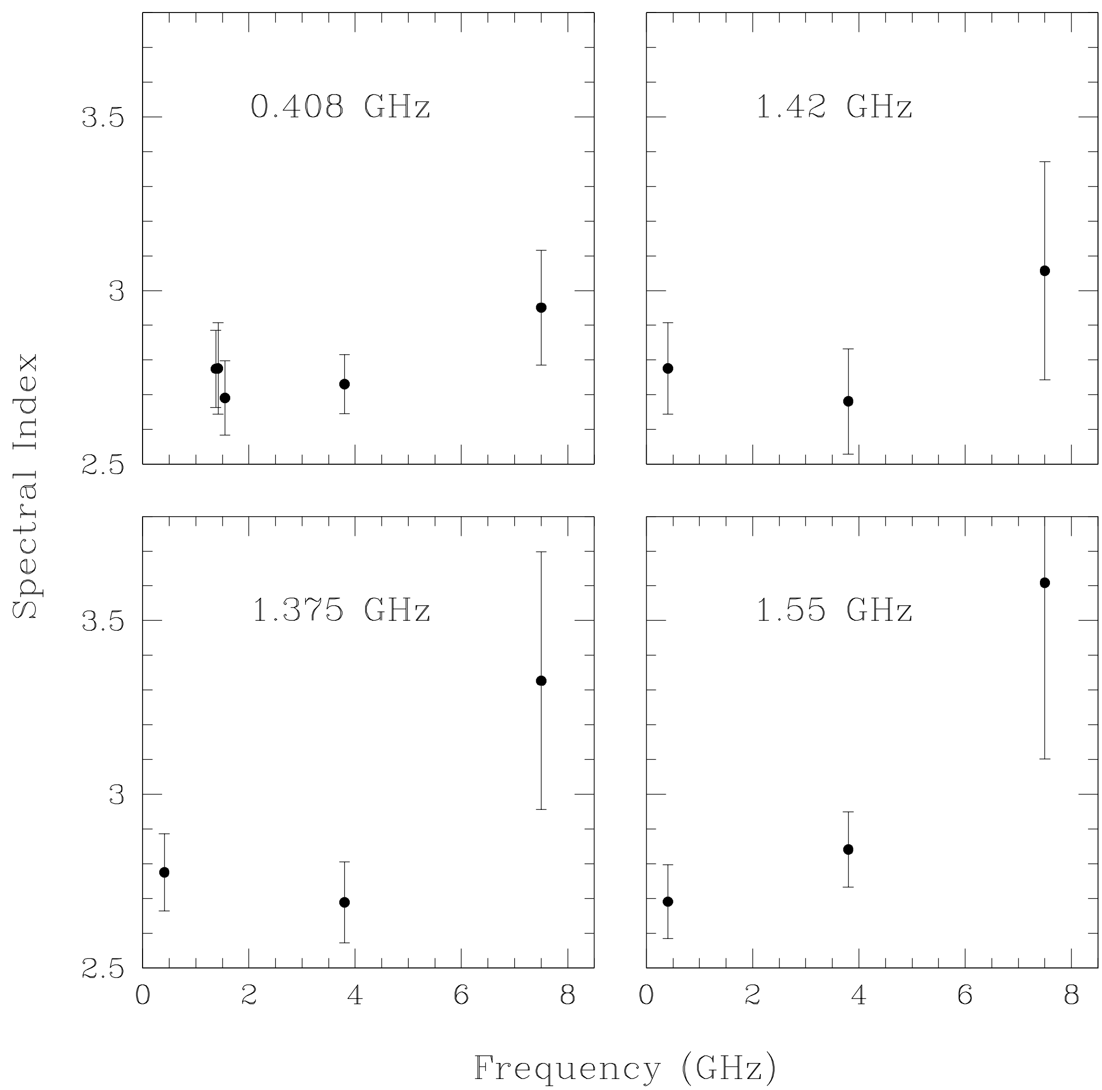

FIG. 4.—Spectral indices. In each box, the spectral indices between the frequency indicated in the box and the frequencies on the x-axis are shown.

Instrumental effects can arise from uncertainties in the beam pattern configuration, errors in the pointing direction, variations of atmospheric emission, and from the possible change of the instrument response when tipped between pointing directions. It is important to point out that for the differential reduction technique we used, an effect that is constant in time or sky position would not affect the estimate of spectral index; in fact, adding a constant value to the data set of an instrument would not change the slope of the fit that is used to calculate β_{syn}. An example of this is the ground contribution, which has not been considered in the analysis.

The uncertainty in the HPBW, as measured during the experiment, is $\pm 2°$. To evaluate the effect on β_{syn}, we used the synthetic sky at each frequency convolved with the nominal beams of the experiment (HPBW = 16°, 17°, 18°, and 21°) and with the same beams but with $\pm 2°$ in the HPBW. The resulting changes in β_{syn} are the errors listed in Table 4 ($\sigma_{\beta,\mathrm{beam}} \lesssim 0.04$).

The measured uncertainty in the pointing directions is $\lesssim 30'$. To estimate the effect of this pointing uncertainty on the spectral index, we constructed TT plots with the Haslam differential profile resulting from two "absolute" profiles corresponding to a 30′ change in pointing direction (i.e., $2^{\mathrm{h}}26^{\mathrm{m}}$ in R.A. instead of $2^{\mathrm{h}}30^{\mathrm{m}}$). The difference between the values of β_{syn} with these two different displacements in R.A. was calculated for every TT plot with 408 MHz data; the resulting mean percentage error is quite small ($\sigma_{\beta,\mathrm{point}} \simeq$ 0.1%), a value also assumed in the TT plots without the Haslam data.

Figure 5 shows correlations between data taken on different days for the frequencies we analyzed; the correlation is very good for the radiometer at the lowest frequency (1.375–1.55 GHz), although less good for the 3.8 GHz com-

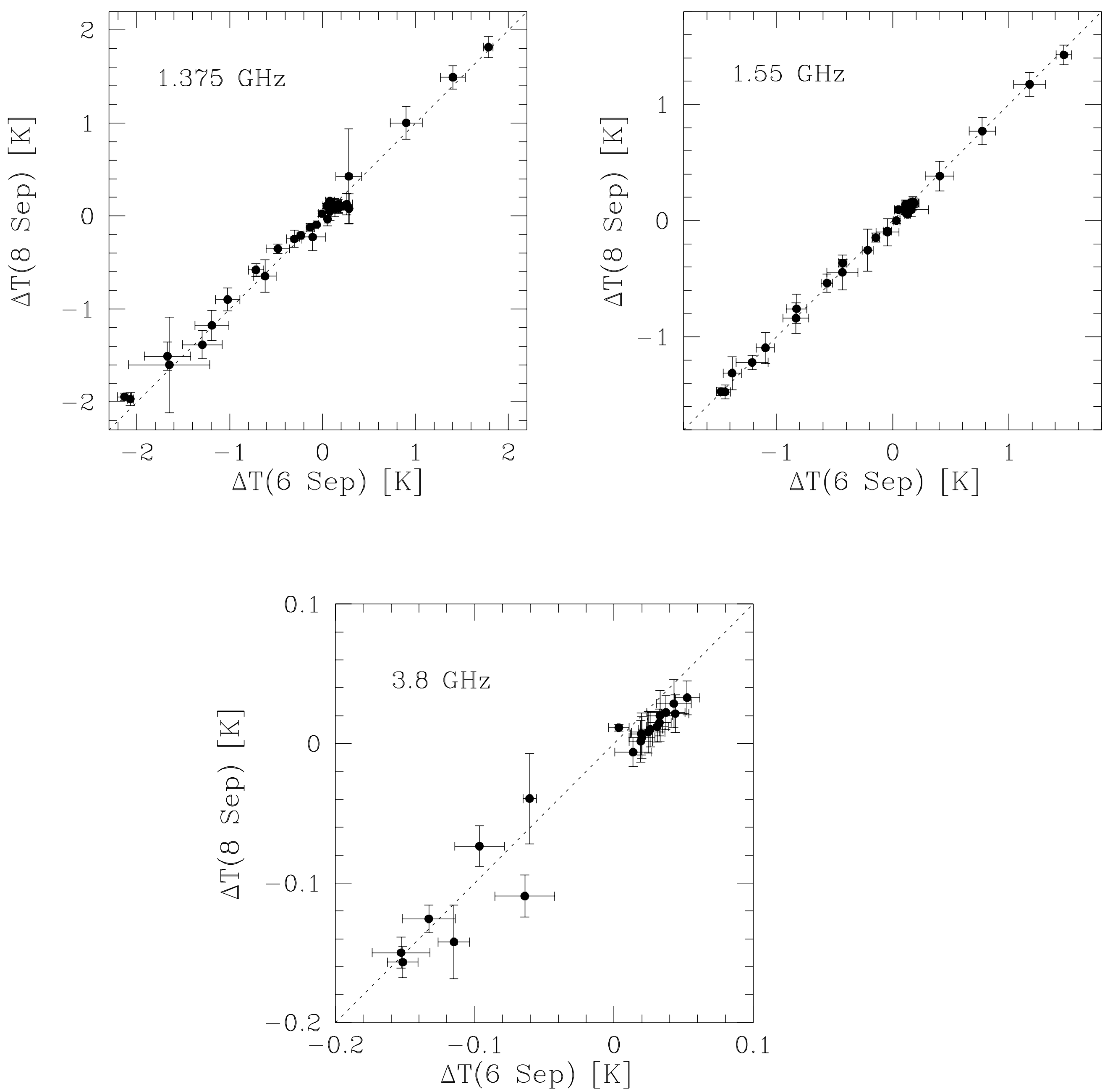

FIG. 5.—Correlations between data taken on different days: *x*-axis plots data taken 1988 Sep. 6, *y*-axis plots data taken Sep. 8.

parison. To evaluate the effect of data nonrepeatability, for each pair of frequencies we made two TT plots using the data registered on 1998 September 6 and 8; using the differences between each pair of β_{syn}, we evaluated a mean percentage error on the synchrotron spectral index (2%). The origin of this effect could lie in the radiometer position dependence, but it may also arise from variations of atmospheric emission. While the water vapor contribution is very small at these frequencies, the overall atmospheric radiation varies with position and time for changes in pressure profiles (Bersanelli et al. 1995a) in a way compatible with the observed variation in our data. We include this effect in $\sigma_{\beta,\mathrm{atm}}$.

The uncertainty in the calibration coefficient G was also considered; the nature of the resulting error is statistical, because it is dominated by the uncertainty on the registered value of the ambient temperature. In Table 4 (typical range $\sim$0.05–0.1), this component is included in the statistical data errors, $\sigma_{\beta,\mathrm{stat}}$, arising from the fitting of the TT plots.

5. DISCUSSION

We have used our results to study the behavior of the synchrotron spectral index with frequency and to evaluate a mean synchrotron spectral index within the frequency range of the experiment (§§ 5.1 and 5.2). The frequency dependence is consistent with that expected from the steepening of the Galactic cosmic-ray electron spectrum. In addition, we have compared the Haslam et al. (1982) map with a map at high frequency (19 GHz) in order to investigate the spatial variations of β_{syn} (§ 5.3).

5.1. *Frequency Variation*

As discussed in § 1, synchrotron radiation arises from cosmic-ray electrons; the interstellar energy spectrum does not have a constant slope, but steepens at an energy of $\sim$10–20 GeV. In fact, cosmic-ray electrons lose energy through different mechanisms: at energies $\lesssim$10–20 GeV they escape from the Galaxy; for $E \gtrsim$ 10–20 GeV, the prevalent mechanism is synchrotron radiation. Because of the two combined effects, the equilibrium spectrum of the electrons changes its slope in this energy range (Webber 1983), corresponding to a frequency of $\sim$10 GHz. Consequently, the synchrotron spectral index, β_{syn}, which is related to the electron spectral index δ, increases with increasing frequency (Lawson et al. 1987; Banday & Wolfendale 1990, 1991). The results of our analysis (Fig. 4) do indeed suggest an increase in β_{syn} corresponding to our highest frequency of 7.5 GHz, although with a relatively poor signal-to-noise ratio. At our lower frequencies, as expected, the spectrum is flatter. In Figure 6, we compare our results with the few previously published results in our frequency range and at higher frequencies (Table 5), and the trend seems to be confirmed.

5.2. *Evaluation of a Mean Synchrotron Spectral Index*

In the frequency range of our measurements, it is possible to evaluate a mean synchrotron spectral index in the observed sky region, since there is not an evident steepening until higher frequencies. A mean β_{syn} between 1.4 and 3.8 GHz has been estimated using the results from the three TT plots between 1.375, 1.550, 1.42, and 3.8 GHz, which are the most statistically significant; the result is $\beta_{syn} = 2.76 \pm 0.09$. Next, we calculate the spectral index using all the results, by a weighted mean of the indices derived with the TT plots;

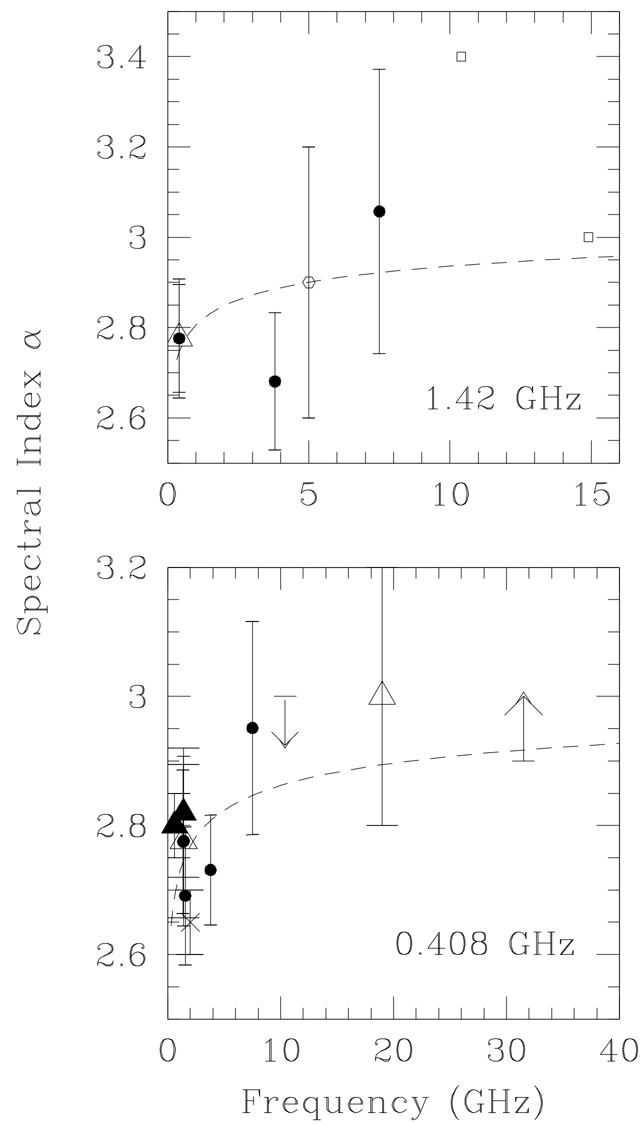

FIG. 6.—Spectral indices derived in this work compared with other published estimates. In the upper plot, indices are between 1.42 GHz and frequencies on the x-axis; in the lower plot, between 0.408 GHz and frequencies on the x-axis. *Filled circles*: This work. *Open triangles*: Our evaluations of β_{syn} from the maps at 0.408, 1.42, and 19 GHz. See Table 5 for references to the other points. The smoothed dashed lines are naive calculation of the spectral index based on the local cosmic-ray electron spectrum.

TABLE 5

OTHER EVALUATIONS OF β_{syn}

Frequency Range (GHz)	β_{syn}	HPBW (deg)	Reference	Notes
0.408–0.610	2.80 ± 0.05	15	1	
0.408–1.407	2.82 ± 0.1	15	1	
0.408–2	2.65 ± 0.05	14	2	$-40 \le \delta \le -60$
0.408–10.4	≤3	5	3	$\delta = +40$
0.408–31.5	≥2.9	7	4[a]	full sky
1.42–5	2.9 ± 0.3	2	5	
1.42–10.4	3.4	5	5	
1.42–14.9	3.0	5	5	

[a] We independently estimated the spectral index between 0.408 and 31 GHz, deriving the same result.

REFERENCES.—(1) Webster 1974; (2) Bersanelli et al. 1995b; (3) Davies et al. 1996; (4) Kogut et al. 1996; (5) COBRA-SAMBA: Report on the Phase A Study, available at: http://www-cosmo.iap.fr/cosa/PUBLIC/report.html.

this is less statistically meaningful because of some redundant information coming from different TT plots (for example, the TT plot between 1.375 and 7.5 and that between 1.375 and 3.8 cover partly the same frequency region), but it gives good information on the behavior of β_{syn} in a larger frequency range. For each index, the error in the weighted mean is the quadratic sum of statistical plus pointing and beam errors (the last two errors have an independent effect on the TT plots). On the other hand, polarization, H II, and atmosphere errors were considered as systematic, since the effects they have on the different evaluations of β_{syn} are not independent. The mean β_{syn} using only our data yields $\beta_{syn} = 2.81 \pm 0.16$; adding data from the 0.408 and 1.42 GHz maps, we derive $\beta_{syn} = 2.76 \pm 0.11$.

5.3. *Spatial Variation*

As we said in § 1.1, the synchrotron spectral index also has a consistent spatial variation because of changes in the electron spectrum and density and changes in the magnetic field intensity with the position in the sky (eq. [3]). Figure 7 shows a TT plot of data from the Haslam et al. (1982) map versus data from a preliminary 19 GHz map (Cottingham 1987; Boughn et al. 1990). The best-fitting line to the data yields an estimate of $\beta_{syn} = 3.01$. However, there is a large range of possible values of β_{syn} compatible with the dispersion of the data; much of the dispersion appears to be correlated with large angular scale spectral variation.

This behavior of β_{syn} is apparent in Figure 8, where we show the ratio between the two maps after subtraction of the CMB signal and the zero level. The 19 GHz offset was estimated by extrapolating the best fit in the 0.408 versus 19 GHz TT plots. If $T_1(i)$ is the temperature of the ith pixel in the 408 MHz map and $T_2(i)$ is the temperature of the same pixel at 19 GHz, the ratio map shows

$$\text{ratio} = \frac{T_2(i)}{T_1(i)} \left(\frac{\nu_2}{\nu_1}\right)^{\beta_{syn}}, \qquad (10)$$

where we fix β_{syn} to a mean value of 2.8. Then, if the synchrotron spectral index changes from this mean value, the pixel color in the map changes, too; an increase in β_{syn} makes the color black, while a decrease leads to red. One can recognize the feature of the North Polar Spur, where the synchrotron spectral index is steeper than the average (Lawson et al. 1987; Reich & Reich 1988). Apart from this feature, the spectrum is flatter than the average at high Galactic latitudes. This is in agreement with Reich & Reich (1988); they found a flattening of the spectrum with increasing latitude in the outer Galaxy direction and also some evidence for a similar effect in the inner Galaxy direction (even if only the north hemisphere data are currently available). In addition, Bloemen et al. (1993) found a hardening of the gamma-ray spectrum with latitude, which translates into a flattening in the radio spectrum. The reason for the hardening of gamma rays is still unclear, since from a simple diffusion model of the cosmic rays (Ginzburg & Syrovatskii 1964) a spectral steepening with latitude is expected. More complex models (e.g., Reich & Reich 1988; Bloemen et al. 1993), such as halo models, may explain the observed effect via a competition of many different mechanisms (spatial diffusion, convection, adiabatic deceleration, and energy losses), but the situation is very complex and needs more data and modeling. Finally, we calculated the synchrotron spectral index between the two

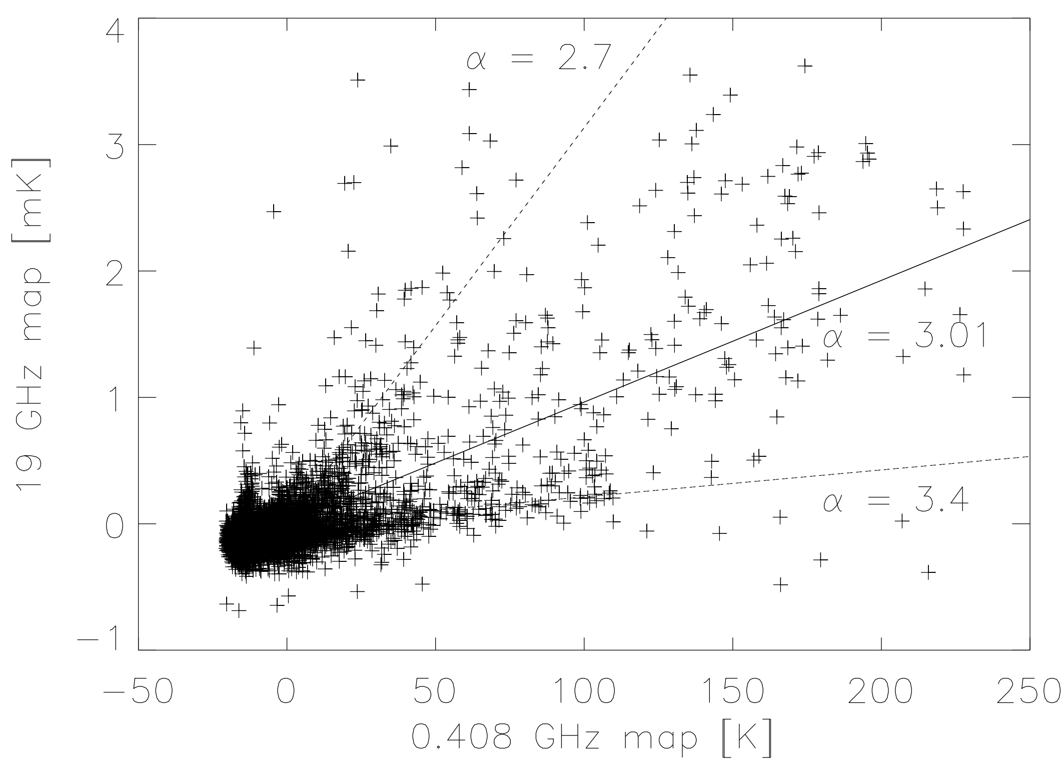

FIG. 7.—TT plot with all-sky data from 408 MHz and 19 GHz maps. In the plot, a best fit to the data is shown (*solid line*), together with upper and lower limits (*dashed lines*) to possible spectral index values. An offset has been subtracted from the 19 GHz data; some 19 GHz and Haslam et al. (1982) data have negative values because the mean has been subtracted to calculate the best fit.

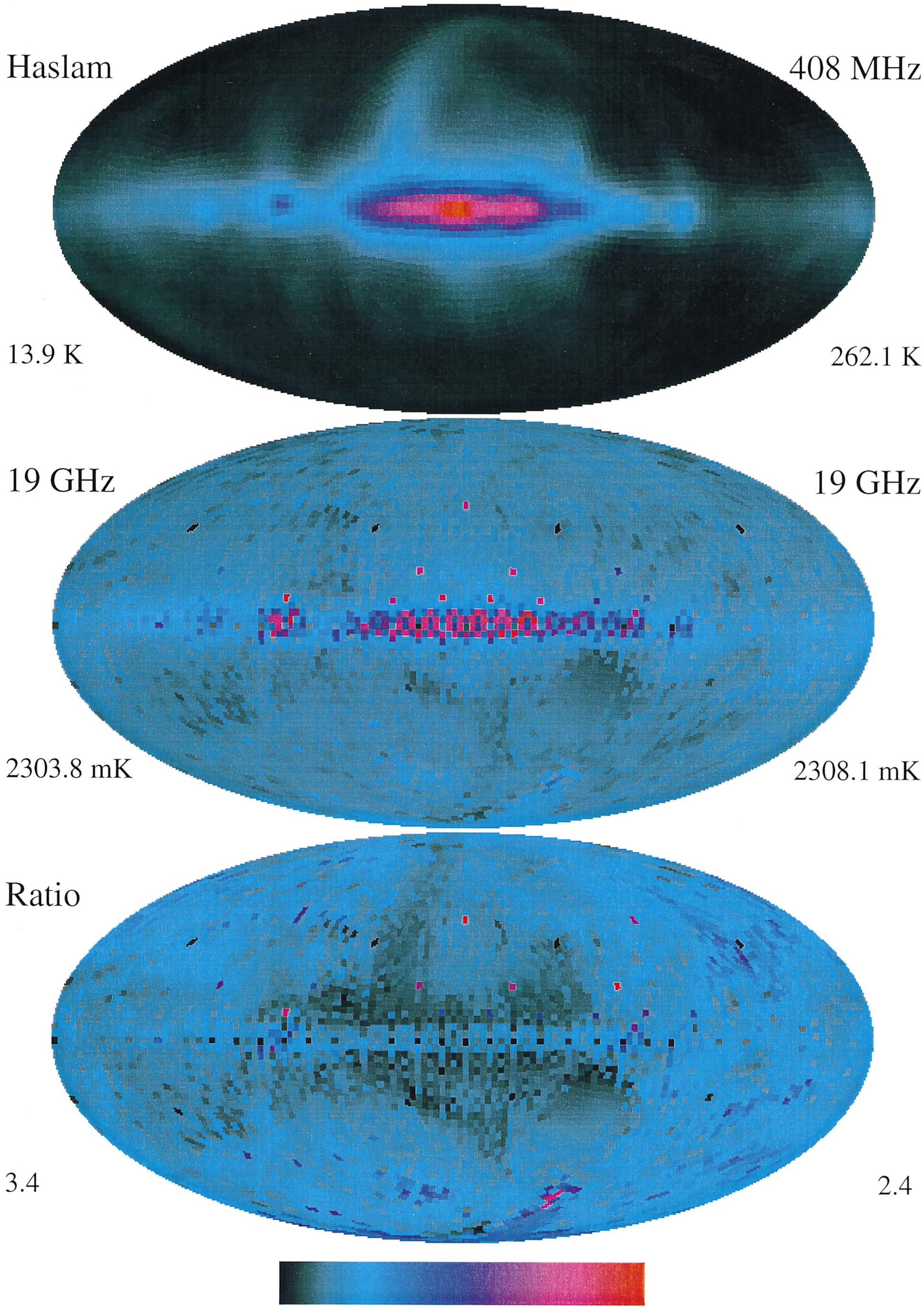

FIG. 8.—*Top*: Haslam et al. (1982) 408 MHz full-sky map. The minimum and maximum temperatures are given below the map. *Center*: Preliminary 19 GHz map (Cottingham 1987; Boughn et al. 1990). The two smoothed regions (one in the southern hemisphere on the right, the other in the northern hemisphere on the left) are not covered by the survey, and the blank pixels have been replaced with the average temperature from surrounding regions. The minimum and maximum temperatures given below the panel include the offset of the survey. *Bottom*: Ratio map between the 0.408 and 19 GHz maps. The numbers below it give the maximum and minimum spectral index.

maps in the celestial region of our experiment to be $\beta_{syn} = 3.00 \pm 0.20$, as shown in Figure 6. The 19 GHz map is preliminary, and because of residual errors in this map the ratio between 19 and 0.408 GHz only gives an indication of the spatial variations of the synchrotron spectral index in that frequency range.

6. CONCLUSIONS

We have analyzed data obtained as part of an experiment dedicated to measuring the centimeter wavelength spectrum of the Galactic continuum emission. The radiometers, operating at 1.375, 1.55, 3.8, and 7.5 GHz, observed a celestial region at declination 36°. The differential reduction technique has allowed us to cancel the first-order contributions from all the isotropic and zenith-symmetric signals received by the radiometers, leaving the Galactic signal. In order to evaluate the synchrotron spectral index, β_{syn}, we have subtracted from the data the H II component derived from a catalog of H II regions. We have used TT plots to calculate the synchrotron spectral index and to evaluate systematic errors (arising from uncertainties in the H II contribution, beam pattern configuration, pointing direction, and atmospheric emission); we have compared our data with the Haslam et al. (1982) and Reich & Reich (1986) maps to yield an estimate of β_{syn} in the frequency range 0.408–7.5 GHz, primarily in the region of the Galactic plane. The general behavior of β_{syn} in this frequency range suggests that a steepening of the synchrotron radiation spectrum at a frequency of ~ 10 GHz is already seen at our higher frequency of 7.5 GHz. The mean value of the synchrotron spectral index is 2.81 ± 0.16 in the frequency range of this experiment (1.375–7.5 GHz), and 2.76 ± 0.11 including the two maps.

As Figure 6 shows, it is important to acquire new, accurate sets of data in the frequency range 1–50 GHz to understand the behavior of the synchrotron spectral index with frequency. In particular, high-sensitivity maps of extended regions of the Galaxy at subdegree angular resolution will be extremely important in the context of the next generation of CMB experiments, such as the two planned space missions *MAP* and *Planck Surveyor*. These two missions will produce high-quality, detailed maps at high frequency and will need high-quality, high-resolution, low-frequency maps to disentangle the synchrotron and free-free emission and to provide the necessary data for understanding these radiations.

We thank L. Danese, E. Gawiser, and C. Paizis for useful discussions and suggestions; we also thank J. Aymon for his technical support and T. Spoelstra for making available the polarization data. We also thank the referee for his help in making this paper much more complete and clear. This work was funded in part by the Collaborative Research Grant CRG960175 of NATO International Scientific Exchange Program and by the Director, Office of Energy Research, Office of High Energy and Nuclear Physics, Division of High Energy Physics of the U.S. Department of Energy, under contract DE-AC03-76SF00098.

REFERENCES

Baars, J. W. M., et al. 1977, A&A, 61, 99
Banday, A. J., & Wolfendale, A. W. 1990, MNRAS, 245, 182
———. 1991, MNRAS, 248, 705
Bennet, C. L., et al. 1992, ApJ, 396, L7
Bensadoun, M., et al. 1993, ApJ, 409, 1
Bersanelli, M., et al. 1995a, ApJ, 448, 8
———. 1995b, Astrophys. Lett. Comm., 32, 7
Bloemen, H., et al. 1993, A&A, 267, 372
Boughn, S. P., et al. 1990, Rev. Sci. Instrum., 61, 158
Brouw, W. N., & Spoelstra, T. A. Th. 1976, A&AS, 26, 129
Cottingham, D. A. 1987, PhD thesis, Princeton Univ.
Davies, R. D., et al. 1996, MNRAS, 278, 925
De Amici, G., et al. 1990, ApJ, 359, 219
Ginzburg, V. L., & Syrovatskii, S. I. 1964, The Origin of the Cosmic Rays (Oxford: Pergamon)
Haslam, C. G. T., et al. 1982, A&AS, 47, 1
Kogut, A., et al. 1990, ApJ, 355, 102
———. 1996, ApJ, 460, 1
Lawson, K. D., et al. 1987, MNRAS, 225, 307
Press, W. H., et al. 1992, Numerical Recipes (2d Ed.; Cambridge: Cambridge Univ. Press)
Reich, P., & Reich, W. 1986, A&AS, 63, 205
———. 1988, A&AS, 74, 7
Scheffler, H., & Elsässer, H. 1987, Physics of the Galaxy and Interstellar Matter (Heidelberg: Springer)
Smoot, G. F., et al. 1985, ApJ, 291, L23
Verschuur, G. L., & Kellermann, K. I., ed. 1988, Galactic and Extragalactic Radio Astronomy (2d Ed.; Berlin: Springer)
Webber, W. R. 1983, in Composition and Origin of Cosmic Rays (Dordrecht: Reidel), 83
Webster, A. S. 1974, MNRAS, 166, 355
Witebsky, C., et al. 1987, IEEE Trans., AP-35, 1310